Strategy for constructing compact numerical atomic orbital basis sets by incorporating the gradients of reference wavefunctions

Peize Lin,[1,2] Xinguo Ren,[3,*] and Lixin He[1,4,†]

[1]*CAS Key Laboratory of Quantum Information, University of Science and Technology of China, Hefei, Anhui 230026, China*

[2]*Songshan Lake Materials Laboratory, Dongguan, Guangdong 523808, China*

[3]*Beijing National Laboratory for Condensed Matter Physics, Institute of Physics, Chinese Academy of Sciences, Beijing 100190, China*

[4]*Synergetic Innovation Center of Quantum Information and Quantum Physics, University of Science and Technology of China, Hefei 230026, China*

(Received 4 March 2021; accepted 2 June 2021; published 15 June 2021)

We develop an algorithm to construct high-quality numerical atomic orbital (NAO) basis sets suitable for large-scale, efficient density-functional calculations. The key idea behind this algorithm is that, in addition to fitting the reference wavefunctions themselves generated by plane-wave based calculations of chosen target systems, the first derivatives of the reference wavefunctions are also taken into account as the fitting target. By doing so, the quality of the generated NAO basis sets is significantly improved in the sense that the same level of numerical precision can be achieved with smaller basis set sizes or with reduced cutoff radii of the NAOs.

DOI: 10.1103/PhysRevB.103.235131

I. INTRODUCTION

In the past decades, numerical atomic orbitals (NAOs) have become a popular choice of basis functions in the first-principles calculations. They are adopted in several newly developed first-principles softwares, such as Dmol [1], SIESTA [2], FPLO [3], FHI-aims [4], OpenMX [5], and others. Compared to another popular basis set, the plane wave (PW) bases, NAO bases are more compact, and usually strictly localized in real space. These properties bring advantages in studying large physical systems, containing hundreds or even thousands of atoms.

However, unlike the PW bases, which can be systematically improved by just increasing the kinetic energy cutoff, the atomic basis sets must be constructed very carefully to ensure both good accuracy and transferability. Furthermore, the quality of the basis sets should be systematically improvable in an unbiased way, which is not trivial to achieve for NAO bases. In the past, several schemes to construct NAOs have been attempted [2,4,5]. For example, one way to construct atomic orbitals is to solve an effective one-electron problem of isolated atoms subject to certain confinement potentials [6,7]. Alternatively, Blum *et al.* proposed a procedure to generate optimized NAO basis sets by picking up iteratively the basis functions one by one from a large pool of *predefined* candidates, so that the weighted sum of ground-state total energies of target systems is improved most of a time [4]. Alternatively, within OpenMX [5], the shape of NAOs is optimized on the fly along with the self-consistency cycle, and consequently the final NAOs are adapted to the specific chemical environment of a given material [5].

In the above methods, the energies have been used as the criterion to generate optimized NAOs. An alternative approach was taken by Chen, Guo, and He (CGH), [8] who proposed a procedure to systematically generate NAOs by fitting them to the high-quality plane-wave calculations for chosen reference systems (usually diatomic molecules), via the spillage formalism [9,10]. It has been demonstrated the generated NAOs using the CGH procedure have very good transferability and can produce reliable results for both isolated and periodic systems [8,11]. In contrast to the NAO bases reported in the literature where the egg-box effects are relatively large [12], the CGH NAO basis sets have very small egg-box effects [11] and therefore allow the forces be converged to very high accuracy during structural relaxations. The CGH bases have been successfully applied in studying the structures of DNA under stretch [13], deuterium diffusion in Li-Sn liquid [14], $AlCl_4$ diffusion in graphite [15], Mg isotope diffusion in $MgSiO_3$ and Mg_2SiO_4 melts [16], the electronic structures of hyperuniform SiO_2 [17], etc.

Despite their success, here we show that the CGH scheme can be further improved to generate NAO bases of higher quality. The key idea behind this improvement is the following. Within the original CGH scheme, only the wavefunctions of the reference systems are fitted. However, we know that the kinetic energies are very sensitive to the derivatives of the wavefunctions, and the derivatives of two wavefunctions could be quite different even if they have large overlap (or small spillage). Therefore, it is natural to ask what happens if the derivatives of the wavefunctions of the reference systems are also taken into account in the fitting procedure, in addition to the wavefunctions themselves. It turns out that the incorporation of the derivatives of the reference wavefunctions indeed helps to improve the quality of the NAOs.

In this work, we present the improved algorithm for basis optimization whereby the derivatives of the reference wavefunctions are incorporated. Benchmark calculations of

*renxg@iphy.ac.cn
†helx@ustc.edu.cn

both molecular and crystalline systems will be presented to assess the quality of the NAO basis sets generated using this algorithm, in comparison to its precedents. We show that the small double-ζ plus polarization (DZP) basis set resulting from this algorithm may yield comparable accuracy to that of the much larger triple-ζ plus double polarization (TZDP) or even quadruple-ζ plus triple polarization (QZTP) bases generated by the old scheme.

The rest of paper is organized as follows. Details of our scheme to construct NAOs are given in Sec. II. We benchmark the quality of the created NAO bases by calculating the structural and electronic properties of a wide variety of systems in Sec. III. We summarize our paper in Sec. IV.

II. METHODS

In Ref. [8], the NAOs are generated by minimizing the "spillage" between the Hilbert space spanned by a set of local basis functions and that spanned by the "exact" wavefunctions of the interested states of the reference systems [9,10]. In this work, we further optimize the NAO bases by taking the wavefunction derivatives into consideration.

We first define an error function between the reference wavefunctions $|\Psi_n\rangle$ and their projected wavefunctions on Hilbert space expanded by the NAO bases $|\tilde{\Psi}_n\rangle$,

$$\Delta_{\mathrm{PSI}} \stackrel{\mathrm{def}}{=} \frac{1}{N_n}\sum_{n=1}^{N_n} \| \, |\Psi_n\rangle - |\tilde{\Psi}_n\rangle \, \|^2, \tag{1}$$

where

$$|\tilde{\Psi}_n\rangle \stackrel{\mathrm{def}}{=} \hat{P}\,|\Psi_n\rangle\,. \tag{2}$$

Here, $\hat{P}$ is the projector spanned by the NAOs, i.e.,

$$\hat{P} = \sum_{\mu\nu} |\phi_\mu\rangle\, S^{-1}_{\mu\nu}\, \langle\phi_\nu|\,, \tag{3}$$

where $\phi_\mu(\mathbf{r})$ is the μth NAO and S^{-1} is the inverse of the overlap matrix $S_{\mu,\nu} \stackrel{\mathrm{def}}{=} \langle\phi_\mu|\phi_\nu\rangle$. Utilizing $\hat{P}^2 = \hat{P}$ and $\langle\Psi_m|\Psi_n\rangle = \delta_{mn}$, it is easy to show that the error function

$$\Delta_{\mathrm{PSI}} = \frac{1}{N_n}\sum_{n=1}^{N_n}\left[1 - \langle\Psi_n|\hat{P}|\Psi_n\rangle\right] \tag{4}$$

is just the "spillage" between the Hilbert space of reference wavefunctions and that spanned by the NAOs [8–10].

In this work, we generalize the definition of this error function by including the derivatives of the wavefunctions. The total error function is now defined as

$$\Delta_{\mathrm{tot}} \stackrel{\mathrm{def}}{=} \frac{1}{N_n}\sum_{n=1}^{N_n}[\||\Psi_n\rangle - |\tilde{\Psi}_n\rangle\|^2 + \||\nabla\Psi_n\rangle - |\nabla\tilde{\Psi}_n\rangle\|^2], \tag{5}$$

where $|\nabla\Psi_n\rangle$ and $|\nabla\tilde{\Psi}_n\rangle$ are the gradients of the reference and projected wavefunctions, respectively. From Eqs. (2) and (3), one may recognize that $|\tilde{\Psi}_n\rangle$ is a linear combination of the NAOs $\{|\phi_\mu\rangle\}$, i.e.,

$$|\tilde{\Psi}_n\rangle = \sum_\mu a_{\mu n}\,|\phi_\mu\rangle\,, \tag{6}$$

with

$$a_{\mu n} = \sum_\nu S^{-1}_{\mu\nu}\,\langle\phi_\nu|\Psi_n\rangle\,. \tag{7}$$

Therefore, the gradient of the projected wavefunctions is also a linear combination of the gradients of the NAOs,

$$|\nabla\tilde{\Psi}_n\rangle = \sum_\mu a_{\mu n}\,|\nabla\phi_\mu\rangle\,. \tag{8}$$

The second term on the right-hand side of Eq. (5) becomes

$$\begin{aligned}&\| \, |\nabla\Psi_n\rangle - |\nabla\tilde{\Psi}_n\rangle \, \|^2 \\ &\quad= \langle\nabla\Psi_n|\nabla\Psi_n\rangle - \sum_\mu a_{\mu n}\,\langle\nabla\Psi_n|\nabla\phi_\mu\rangle \\ &\qquad- \sum_\nu a^*_{\nu n}\,\langle\nabla\phi_\nu|\nabla\Psi_n\rangle + \sum_{\mu\nu} a_{\mu n}a^*_{\nu n}\,\langle\nabla\phi_\nu|\nabla\phi_\mu\rangle\,.\end{aligned} \tag{9}$$

The inner products of the gradients are calculated in reciprocal space, e.g.,

$$\langle\nabla\phi_\nu|\nabla\phi_\mu\rangle = \sum_{\mathbf{G}} |\mathbf{G}|^2\phi^*_\nu(\mathbf{G})\phi_\mu(\mathbf{G}), \tag{10}$$

where $\phi_\mu(\mathbf{G}) \stackrel{\mathrm{def}}{=} \langle\mathbf{G}|\phi_\mu\rangle$ is the Fourier transform of $\phi_\mu(\mathbf{r})$ in the reciprocal space.

The NAOs are given by numerically tabulated radial functions multiplied by spherical harmonic functions, $\varphi_{\alpha l\xi m}(\mathbf{r}) \stackrel{\mathrm{def}}{=} f_{\alpha l\xi}(r)Y_{lm}(\hat{r})$, where α is the element type, ζ is the multiplicity of the radial functions for the angular momentum l, and m is the magnetic quantum number. The basis function $\phi_\mu(\mathbf{r})$ is $\phi_{\alpha il\xi m}(\mathbf{r}) = \varphi_{\alpha l\xi m}(\mathbf{r} - \tau_{\alpha i})$, where i is the index of the atom of αth element and $\tau_{\alpha i}$ is the atom position. Following the CGH scheme [8], the radial functions are expanded as linear combinations of spherical Bessel functions, i.e.,

$$f_{\alpha l\xi}(r) = \begin{cases}\sum_q c_{\alpha l\xi q}\, j_l(qr), & r < R_c,\\ 0, & r \geqslant R_c.\end{cases} \tag{11}$$

Here $j_l(qr)$ is the spherical Bessel function and q is chosen to satisfy $j_l(qR_c) = 0$, where R_c is the cutoff radii of the radial functions, beyond which the NAOs are strictly zero. The number of spherical Bessel functions [controlled by the highest q in Eq. (11)] are determined by the same energy cutoff of plane wave calculations.

To generate optimized and transferable NAOs, we choose for each element a group of dimers at different bond lengths as the reference systems. We perform high-quality plane wave calculations for these reference systems, and use the obtained Kohn-Sham molecular wavefunctions as the reference wavefunctions. The average error functions are then evaluated using Eq. (1) or (5), following the procedure proposed in Ref. [8]. Previous works [4,11] demonstrate that the NAO bases generated according to these reference systems have remarkable transferability, which may be used for complex chemical environment, including defects, surfaces, alloys, etc.

The coefficients $c_{\alpha l\xi q}$ in Eq. (11) are determined by minimizing the error functions between the reference wavefunctions and projected wavefunctions as defined in Eq. (5). To calculate the gradients of the error function $\partial\Delta_{\mathrm{tot}}/\partial c_{\alpha l\xi q}$, we use the automatic differentiation techniques as implemented in PyTorch [18]. The error function is then minimized via Adam algorithm [19]. This approach is orders of magnitude faster than the simulated annealing method used in Ref. [8].

TABLE I. Radial basis functions of the hierarchical basis set SZ, DZ, DZP, TZDP, and QZTP for 24 different chemical elements used in this paper. The SZ basis prescription also reflects the valence electrons of the employed pseudopotentials behind.

Element	SZ	DZ	DZP	TZDP	QZTP
H	$1s$	$2s$	$2s1p$	$3s2p$	$4s3p$
Li	$2s$	$4s$	$4s1p$	$6s2p$	$8s3p$
B C N O F Si P S Cl As Se Br	$1s1p$	$2s2p$	$2s2p1d$	$3s3p2d$	$4s4p3d$
Na Mg	$2s1p$	$4s2p$	$4s2p1d$	$6s3p2d$	$8s4p3d$
Al	$2s2p$	$4s4p$	$4s4p1d$	$6s6p2d$	$8s8p3d$
Ga In Sb Te I	$1s1p1d$	$2s2p2d$	$2s2p2d1f$	$3s3p3d2f$	$4s4p4d3f$
Zn Cd	$2s1p1d$	$4s2p2d$	$4s2p2d1f$	$6s3p3d2f$	$8s4p4d3f$

In the original CGH work, a smooth function is applied after the generation of the NAOs to make the second derivative of the NAOs continuous near the R_c [8,20]. Furthermore, an extra step is taken to optimize the shapes of the orbitals, by minimizing the kinetic energy of the orbitals. However, we find that these extra steps are no longer needed in the current algorithm, apparently due to the fact that the first derivatives of the reference wavefunctions are also fitted.

It should be mentioned that we also tried to include the second and third derivatives in the definition of the error functions. However, the obtained results are worse than the ones which only involve the first derivatives.

Our NAO basis can be seen as a contraction of spherical Bessel functions, as is evident from Eq. (11). The set of spherical Bessel functions within an energy cutoff, multiplied with spherical harmonics below certain angular momentum themselves represent a basis set. This basis set, which is referred to as jY basis in this paper, represents the upper limit of the accuracy that a NAO basis can achieve for a given maximum angular momentum and radius. This basis is of little value in practical calculations because the size of the basis is too large, but it can be used to benchmark the NAO bases and help us understand the source of error for the NAO bases.

III. RESULTS AND DISCUSSION

In this section, we benchmark the optimized NAO bases for various systems including molecules and crystals. We compare the results obtained by PSI and DPSI bases to the results of PW bases. Here, for convenience, we use "PSI " to denote the old NAO bases and "DPSI " to denote the new ones where the first derivative is involved in the optimization. Both PSI and DPSI basis sets form a hierarchy, ranging from double-ζ (DZ), double-ζ plus polarization functions (DZP), triple-ζ plus double polarization functions (TZDP), to quadrupole-ζ plus triple polarization functions (QZTP). In the present work, the hierarchical NAO basis sets are constructed based on the SG15 pseudopotentials [21], and the size of the actual basis sets for a given chemical element depends on the valence electrons in such a pseudopotential prescription. For example, for Si, the single-ζ (SZ) basis is $1s1p$, whereby one valence electron is described by only one radial basis function. This number is doubled in the DP basis set (i.e., $2s2p$), and in DZP one additional radial function of higher momentum ($l = 2$) is

TABLE II. Cutoff radii R_c (in Bohr) parameters of the LCAO basis functions for 24 different elements used in this paper.

Element	R_c	Element	R_c	Element	R_c
H	8.0	Mg	9.0	As	8.0
Li	9.0	Al	9.0	Se	8.0
B	8.0	Si	8.0	Br	8.0
C	8.0	P	8.0	Cd	9.0
N	8.0	S	8.0	In	9.0
O	7.0	Cl	8.0	Sb	9.0
F	7.0	Zn	9.0	Te	9.0
Na	10.0	Ga	9.0	I	8.0

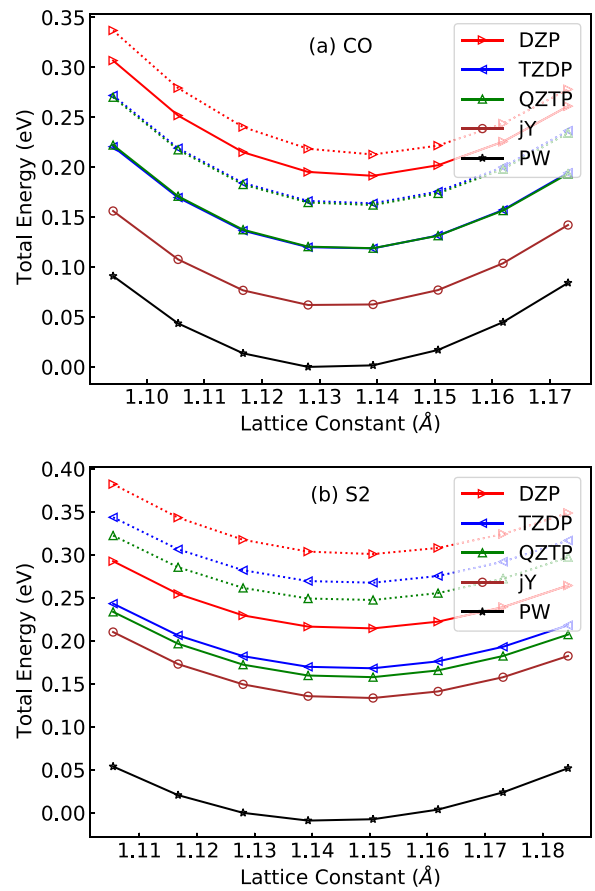

FIG. 1. Comparison of the total energies of CO and S_2 as a function of the bond lengths using different LCAO basis sets to those using the PW and jY bases. The solid and dotted lines represent DPSI and PSI results, respectively.

TABLE III. Total energies (in eV) of 11 molecules obtained with various LCAO basis sets, in comparison with jY and PW. For each molecule, the same structure is used for different basis sets. The total energies of the PW basis are set to zero.

	PSI				DPSI				
	DZ	DZP	TZDP	QZTP	DZ	DZP	TZDP	QZTP	jY
Br_2	1.05	0.28	0.27	0.25	0.98	0.21	0.19	0.18	0.15
Cl_2	1.53	0.26	0.24	0.22	1.50	0.23	0.20	0.18	0.16
CO	1.58	0.22	0.17	0.16	1.55	0.20	0.12	0.12	0.06
F_2	0.65	0.17	0.15	0.13	0.63	0.14	0.11	0.11	0.08
I_2	0.56	0.35	0.33	0.30	0.41	0.14	0.12	0.11	0.07
Li_2	0.41	0.47	0.44	0.38	0.27	0.11	0.11	0.11	0.11
LiH	0.48	0.14	0.13	0.10	0.44	0.07	0.06	0.04	0.02
N_2	1.55	0.15	0.10	0.10	1.54	0.13	0.09	0.08	0.06
Na_2	0.23	0.21	0.17	0.15	0.08	0.07	0.06	0.06	0.09
O_2	1.55	0.25	0.22	0.22	1.51	0.20	0.16	0.15	0.10
S_2	2.02	0.32	0.28	0.26	1.93	0.23	0.18	0.17	0.15
MAE (jY)	0.94	0.14	0.12	0.10	0.89	0.07	0.04	0.03	
MAE (PW)	1.06	0.26	0.23	0.21	0.99	0.16	0.13	0.12	0.10

added, ending up with $2s2p1d$ basis set for Si. The meanings of TZDP and QZTP follow naturally according to this nomenclature. In Table I, the actual sets of radial functions under the acronyms SZ, DZP, DZDP, and QZTP are presented for all the 24 chemical elements used in the present work. The cutoff radii for the different radial basis functions are chosen to be the same for a given chemical element, and these are presented in Table II. For molecules, we also compare the results to those obtained by using jY bases. The jY bases are, however, overcomplete for closely packed crystals, and therefore not used in the comparison.

All calculations are performed by using the ABACUS code. Generalized gradient approximation of Perdew, Burke, and Ernzerhof (PBE) [22] is used as the exchange-correlation functional and, as implied above, the SG15 [21] optimized norm conserving Vanderbilt-type (ONCVP) pseudopotentials [23,24] are employed to represent the ion cores and core-valence interaction. For molecules, the supercell approach with a single Γ point is used, where, for crystals, an $8 \times 8 \times 8$ Monkhorst-Pack (MP) **k**-point mesh is used for the Brillouin zone sampling.

A. Molecules

1. Total energies

Figures 1(a) and 1(b) depict the ground state energies as a function of bond lengths around the equilibrium for the CO and S_2 molecules, respectively, using different basis sets. The results of the DZP, TZDP, and QZTP bases are shown in red, blue, and green, respectively. The dotted lines correspond to the results obtained using the PSI bases, whereas the solid lines represent those obtained using the DPSI bases. The jY (brown solid line) and PW (black solid line) results are also shown as the references. The total energies systematically converge to the jY and PW results as the size of the NAO basis set increases [11]. However, the total energies calculated using

TABLE IV. Bond lengths (in Å) of 11 diatomic molecules obtained with various LCAO basis sets, in comparison with jY and PW.

	PSI				DPSI					
	DZ	DZP	TZDP	QZTP	DZ	DZP	TZDP	QZTP	jY	PW
Br_2	2.4432	2.3261	2.3249	2.3250	2.4421	2.3240	2.3250	2.3247	2.3259	2.3140
Cl_2	2.1904	2.0273	2.0262	2.0278	2.1914	2.0253	2.0266	2.0266	2.0277	2.0149
CO	1.1604	1.1379	1.1355	1.1355	1.1592	1.1365	1.1345	1.1348	1.1332	1.1324
F_2	1.4734	1.4261	1.4227	1.4223	1.4710	1.4222	1.4206	1.4209	1.4215	1.4171
I_2	2.7267	2.6996	2.6962	2.6965	2.7335	2.6973	2.6941	2.6934	2.6928	2.6910
Li_2	2.8379	2.6597	2.6637	2.6650	2.8229	2.7073	2.7066	2.7070	2.7067	2.7284
LiH	1.6497	1.5970	1.6003	1.5961	1.6544	1.6009	1.6037	1.5999	1.6060	1.6081
N_2	1.1234	1.1056	1.1033	1.1031	1.1225	1.1046	1.1028	1.1026	1.1024	1.1017
Na_2	3.0495	3.0576	3.0598	3.0617	3.0653	3.0674	3.0707	3.0709	3.0717	3.0888
O_2	1.2817	1.2241	1.2209	1.2221	1.2808	1.2219	1.2208	1.2211	1.2215	1.2190
S_2	2.0635	1.9224	1.9208	1.9204	2.0624	1.9211	1.9204	1.9208	1.9212	1.9143
MAE (jY)	0.0740	0.0086	0.0066	0.0067	0.0716	0.0025	0.0011	0.0013		
MRE (jY)	3.90%	0.40%	0.28%	0.29%	3.81%	0.14%	0.06%	0.08%		
MAE (PW)	0.0772	0.0160	0.0134	0.0137	0.0748	0.0089	0.0077	0.0080	0.0075	
MRE (PW)	4.08%	0.73%	0.58%	0.60%	3.99%	0.42%	0.35%	0.37%	0.34%	

TABLE V. Atomization energies (in eV) of 11 molecules obtained with various LCAO basis sets, in comparison with jY and PW.

	PSI				DPSI					
	DZ	DZP	TZDP	QZTP	DZ	DZP	TZDP	QZTP	jY	PW
Br_2	1.61	2.21	2.23	2.24	1.61	2.21	2.23	2.24	2.26	2.38
Cl_2	1.70	2.59	2.61	2.63	1.70	2.58	2.61	2.63	2.64	2.78
CO	10.31	11.62	11.67	11.67	10.31	11.60	11.67	11.67	11.70	11.75
F_2	1.97	2.40	2.41	2.42	1.97	2.40	2.42	2.43	2.43	2.51
I_2	1.82	2.04	2.05	2.06	1.78	2.03	2.05	2.06	2.08	2.08
Li_2	0.84	1.16	1.13	1.10	0.78	0.92	0.92	0.92	0.91	0.86
LiH	2.06	2.58	2.57	2.55	2.00	2.35	2.36	2.38	2.39	2.33
N_2	8.52	9.88	9.92	9.92	8.52	9.88	9.92	9.92	9.93	9.99
Na_2	0.85	0.85	0.84	0.83	0.79	0.80	0.80	0.80	0.80	0.77
O_2	5.36	6.49	6.53	6.53	5.36	6.50	6.53	6.55	6.56	6.65
S_2	3.63	4.94	4.98	5.00	3.62	4.94	4.98	4.99	5.00	5.11
MAE (jY)	0.738	0.084	0.056	0.047	0.752	0.046	0.020	0.014		
MRE (jY)	17.73%	4.83%	3.77%	3.18%	18.36%	1.33%	0.70%	0.50%		
MAE (PW)	0.791	0.157	0.128	0.119	0.803	0.111	0.086	0.083	0.072	
MRE (PW)	18.70%	7.75%	6.68%	6.06%	19.11%	3.69%	3.20%	3.14%	2.77%	

the DPSI bases are significantly better than those calculated using the PSI bases of the same size. For S_2, the total energies calculated using the DZP basis of DPSI are even lower than those of the much larger QZTP basis of PSI.

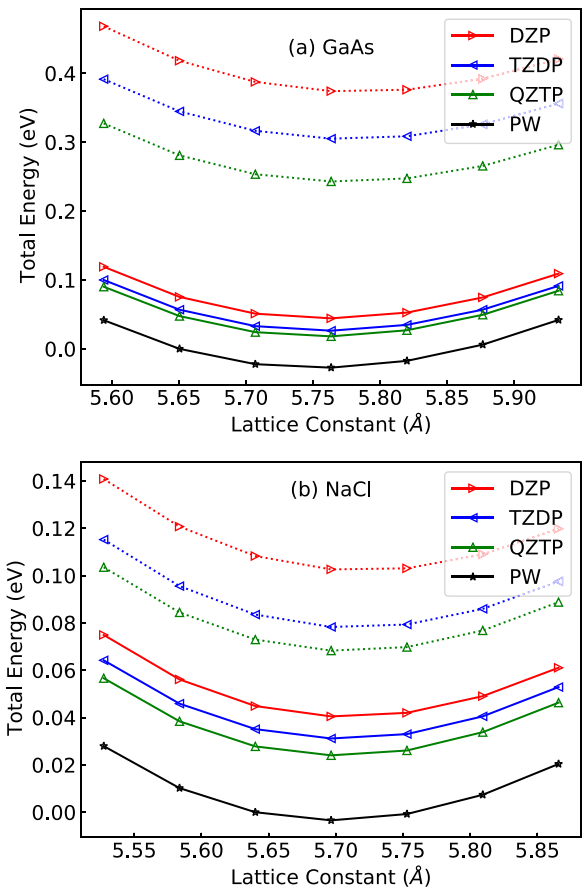

FIG. 2. Total energies of GaAs and NaCl as a function of the lattice constant using different LCAO basis sets, in comparison to the results obtained using the PW basis. The solid lines correspond to the DPSI results and the dotted lines the PSI results.

The total energies of 11 molecules relative to those of PW bases are presented in Table III for different bases. The calculations are done using the same diatomic distance of each

TABLE VI. Total energies (in eV) of 26 solids obtained from various LCAO basis sets, compared to the PW. Each molecule for different basis sets has the same structure. The total energies of the PW basis are set to zero.

	PSI				DPSI			
	DZ	DZP	TZDP	QZTP	DZ	DZP	TZDP	QZTP
AlAs	1.06	0.35	0.32	0.28	0.69	0.10	0.08	0.07
AlNw	2.33	0.79	0.51	0.40	2.10	0.43	0.28	0.25
AlP	1.20	0.35	0.29	0.27	0.87	0.11	0.09	0.08
AlSb	0.74	0.30	0.24	0.21	0.45	0.07	0.06	0.05
BN	0.51	0.13	0.09	0.07	0.46	0.08	0.06	0.05
BP	1.27	0.24	0.19	0.17	1.09	0.10	0.08	0.07
C	0.64	0.10	0.08	0.07	0.60	0.08	0.06	0.05
CdSew	0.99	0.64	0.49	0.43	0.73	0.48	0.19	0.16
CdSw	1.07	0.61	0.44	0.38	0.87	0.33	0.20	0.16
CdTe	0.33	0.25	0.18	0.15	0.21	0.12	0.07	0.06
GaAs	0.67	0.42	0.34	0.28	0.28	0.08	0.06	0.05
GaN	0.53	0.40	0.29	0.25	0.23	0.08	0.05	0.04
GaP	0.81	0.40	0.33	0.28	0.43	0.08	0.06	0.05
GaSb	0.44	0.33	0.26	0.20	0.12	0.05	0.04	0.03
InP	0.72	0.41	0.33	0.29	0.41	0.09	0.07	0.06
LiF	0.35	0.12	0.08	0.07	0.43	0.10	0.09	0.08
MgO	0.51	0.29	0.21	0.15	0.45	0.14	0.10	0.08
MgS	0.63	0.24	0.21	0.16	0.49	0.10	0.08	0.06
NaCl	0.16	0.11	0.08	0.07	0.10	0.04	0.04	0.03
Si	1.55	0.42	0.31	0.30	1.16	0.11	0.09	0.08
SiC	1.74	0.32	0.23	0.20	1.61	0.19	0.14	0.12
ZnO	0.44	0.38	0.23	0.17	0.28	0.17	0.09	0.07
ZnOw	0.89	0.76	0.46	0.34	0.57	0.35	0.17	0.14
ZnS	0.66	0.39	0.25	0.18	0.45	0.16	0.09	0.07
ZnSe	0.59	0.41	0.28	0.20	0.35	0.24	0.09	0.07
ZnTe	0.39	0.33	0.20	0.14	0.18	0.10	0.06	0.04
MAE	0.82	0.36	0.27	0.22	0.60	0.15	0.09	0.08

TABLE VII. Lattice constant (in Å) of 22 fcc solids obtained from various LCAO basis sets, compared to the PW.

	PSI				DPSI				
	DZ	DZP	TZDP	QZTP	DZ	DZP	TZDP	QZTP	PW
AlAs	5.836	5.748	5.742	5.740	5.802	5.741	5.739	5.738	5.733
AlP	5.611	5.522	5.510	5.507	5.593	5.516	5.512	5.511	5.507
AlSb	6.319	6.244	6.237	6.234	6.283	6.228	6.225	6.225	6.224
BN	3.639	3.625	3.623	3.622	3.636	3.623	3.622	3.622	3.621
BP	4.646	4.552	4.549	4.547	4.634	4.547	4.546	4.545	4.541
C	3.586	3.567	3.568	3.568	3.584	3.567	3.569	3.569	3.568
CdTe	6.677	6.648	6.636	6.633	6.667	6.637	6.632	6.630	6.624
GaAs	5.822	5.784	5.778	5.774	5.788	5.759	5.759	5.757	5.753
GaN	4.583	4.580	4.570	4.568	4.573	4.557	4.555	4.554	4.551
GaP	5.595	5.533	5.522	5.521	5.564	5.514	5.513	5.512	5.509
GaSb	6.263	6.246	6.238	6.231	6.236	6.219	6.218	6.217	6.216
InP	6.040	5.984	5.974	5.972	6.023	5.970	5.970	5.969	5.963
LiF	4.117	4.075	4.069	4.067	4.124	4.068	4.069	4.069	4.062
MgO	4.284	4.282	4.270	4.264	4.277	4.268	4.262	4.259	4.256
MgS	5.299	5.243	5.238	5.232	5.287	5.228	5.227	5.226	5.225
NaCl	5.744	5.720	5.715	5.710	5.730	5.709	5.705	5.704	5.699
Si	5.605	5.492	5.486	5.483	5.594	5.481	5.480	5.479	5.476
SiC	4.483	4.393	4.388	4.385	4.475	4.390	4.388	4.386	4.380
ZnO	4.658	4.645	4.633	4.630	4.650	4.632	4.623	4.621	4.616
ZnS	5.558	5.489	5.466	5.461	5.537	5.467	5.456	5.454	5.446
ZnSe	5.829	5.784	5.764	5.752	5.806	5.785	5.752	5.749	5.739
ZnTe	6.241	6.226	6.205	6.194	6.220	6.197	6.188	6.187	6.181
MAE	0.070	0.022	0.013	0.009	0.054	0.010	0.005	0.004	
MRE	1.33%	0.41%	0.25%	0.18%	1.04%	0.19%	0.10%	0.08%	

molecule for all basis sets. Since the absolute value of the total energy is irrelevant, here we set the total energy obtained using the PW bases to zero, and only the energy differences to the PW results are reported. Thus the presented total energy values of the NAO bases can be seen as the basis set errors with respect to the PW reference. In all cases, the errors of total energy (relative to the PW bases) of the DPSI bases are much smaller than those of the PSI bases at the same level. For most of the molecules, errors of the DZP bases for the DPSI type are similar or even smaller than those of the QZTP bases of the PSI type. The errors of the QZTP-DPSI bases are very close to those of the jY bases. The mean absolute error (MAE) relative to both the jY and PW bases are shown at the bottom of Table III. The MAE to jY bases is only 0.07 eV for DZP-DPSI, and 0.03 eV for QZTP-DPSI, which are much smaller than those of the PSI bases at the same level. The MAE of the DPSI bases to the PW results are also much smaller than that of the PSI bases. The MAE of DZP-DPSI is about 0.16 eV smaller than the MAE of QZTP-PSI 0.21 eV to the PW basis.

Importantly, we note that the MAE of the jY basis to the PW basis is already 0.10 eV, which is larger than the MAE between DPSI basis and jY basis. This result suggests that the MAE between DPSI and PW is dominated by the incompleteness of the jY basis, due to the finite cutoff radii [R_c in Eq. (11)] and the maximum angular momentum. As a result, the MAE between DPSI and PW dose not reduce much from DZP-DPSI to QZTP-DPSI bases. Therefore, further increasing the number of radial functions could not significantly improve the results. To further improve the quality of the bases, one has to increase the radii and maximum angular momentum of the NAO bases.

To gain further insights into the origin of why the DSPI bases show a substantial supremacy with respect to the PSI bases, in Tables XII and XIII of Appendix, we present the errors of DZP-PSI and DZP-DPSI bases (with respect to the jY reference results) for individual contributions to the total energy, i.e., the kinetic energy, the potential energies due to local and nonlocal pseudopotentials, and the Hartree and exchange-correlation energies. While Table XII presents the error analysis of individual contributions after the first iteration of the self-consistent calculations, Table XIII presents the counterparts at full self-consistency. This study reveals that the key reason behind the better accuracy of the DPSI bases is their improved wavefunction gradients. This will immediately lead to an improved accuracy in the kinetic energy, which further triggers an improvement in other parts of the total energy through the self-consistent process. Thus it is really the detailed shapes of the entire radial functions that result in the improved quality of the DPSI bases.

2. Bond lengths

Table IV compares the bond lengths of the 11 molecules calculated by different base sets. The bond lengths calculated by DPSI bases are much better than those by PSI bases of the same level. The MAE of the DZP-DPSI bases to the PW bases is 0.0089 Å, much smaller than the MAE of the QZTP-PSI bases 0.0137 Å. The MAEs of DPSI bases to the jY basis (0.0016–0.0028 Å) are extremely small, suggesting that the

TABLE VIII. Cohesive energies (in eV/atom) of 26 solids obtained from various LCAO basis sets, compared to the PW.

	PSI				DPSI				
	DZ	DZP	TZDP	QZTP	DZ	DZP	TZDP	QZTP	PW
AlAs	3.353	3.687	3.705	3.714	3.386	3.665	3.671	3.675	3.651
AlNw	5.158	5.531	5.600	5.618	5.142	5.547	5.583	5.590	5.615
AlP	3.685	4.086	4.113	4.119	3.725	4.081	4.092	4.095	4.083
AlSb	3.118	3.319	3.333	3.337	3.135	3.312	3.316	3.318	3.289
BN	6.641	6.825	6.843	6.852	6.632	6.816	6.823	6.828	6.835
BP	4.822	5.311	5.333	5.342	4.826	5.294	5.304	5.308	5.308
C	7.351	7.612	7.618	7.623	7.350	7.608	7.612	7.615	7.620
CdSew	2.177	2.253	2.279	2.289	2.174	2.227	2.286	2.293	2.305
CdSw	2.423	2.519	2.553	2.560	2.420	2.531	2.561	2.569	2.586
CdTe	1.966	1.998	2.024	2.027	1.969	2.007	2.028	2.032	2.036
GaAs	2.987	3.105	3.136	3.142	3.028	3.123	3.127	3.130	3.096
GaN	4.106	4.163	4.212	4.211	4.178	4.250	4.260	4.262	4.248
GaP	3.250	3.437	3.467	3.468	3.311	3.475	3.480	3.483	3.458
GaSb	2.831	2.878	2.890	2.892	2.859	2.893	2.893	2.893	2.858
InP	3.018	3.149	3.148	3.157	2.982	3.123	3.133	3.136	3.105
LiF	4.355	4.563	4.566	4.547	4.260	4.416	4.420	4.427	4.418
MgO	4.954	5.058	5.079	5.105	4.904	5.051	5.069	5.081	5.088
MgS	3.579	3.757	3.760	3.777	3.554	3.740	3.750	3.756	3.755
NaCl	3.121	3.136	3.136	3.132	3.083	3.108	3.113	3.116	3.100
Si	4.074	4.614	4.645	4.661	4.042	4.521	4.528	4.530	4.494
SiC	5.675	6.355	6.387	6.404	5.618	6.289	6.307	6.314	6.326
ZnO	3.474	3.497	3.564	3.595	3.517	3.564	3.606	3.615	3.631
ZnOw	3.482	3.506	3.573	3.603	3.525	3.572	3.614	3.623	3.639
ZnS	2.694	2.807	2.871	2.906	2.749	2.878	2.910	2.920	2.935
ZnSe	2.386	2.466	2.518	2.557	2.440	2.488	2.555	2.563	2.573
ZnTe	2.118	2.141	2.194	2.216	2.165	2.200	2.220	2.225	2.227
MAE	0.212	0.058	0.045	0.041	0.204	0.033	0.019	0.016	
MRE	5.26%	1.74%	1.24%	1.07%	4.88%	1.00%	0.54%	0.46%	

accuracy is approaching the limit of the NAOs for the given highest angular momentum and cutoff radii of the NAOs. The mean relative error (MRE) of DPSI bases to both the jY and PW bases is also much smaller than that of PSI.

3. Atomization energies

The atomization energies of the 11 molecules are presented in Table V. In this case, the differences between the PSI base and DPSI bases are much smaller than those of the corresponding total energies, which is presumably due to the error cancellation (between the total energies of the molecules and free atoms) in calculating the atomization energies. For many molecules, the atomization energies calculated by the two base sets are very close. However, for some molecules, e.g., Li_2, LiH, and Na_2, the atomization energies calculated by the DPSI bases are significantly better than those by the PSI bases. The overall MAEs of the DPSI bases to the PW bases are much smaller than those of the PSI bases. Again, the MAEs of DPSI bases to the jY bases are already very small, much smaller than the MAE of the jY bases to the PW bases. Therefore, the improvement of the atomization energies is relatively small when increasing the base size from DZP-DPSI to QZTP-DPSI bases.

B. Crystals

After comparing the accuracy of DPSI bases with the PSI bases for the molecules, we turn to the benchmark of their performance for periodic systems. To this end, a set of 26 crystalline solids are chosen as the test systems that cover semiconductors, alkaline and alkaline-earth metals, alkaline chloride, and transition metals. Among them, 22 materials have the face-centered cubic (fcc) structure, whereas four have the wurtzite structure, labeled with a character "w" after the name. For the crystals, the jY bases are too large and overcomplete, which causes serious numerical instability, and therefore are not included in the comparison. We only compare the results of NAOs with the PW bases.

1. Total energies

The total energies as a function of lattice constant for GaAs and NaCl are shown in Figs. 2(a) and 2(b), respectively, for various NAO bases, compared to those of the PW bases. The advantage of the DPSI bases over the PSI ones is remarkable. For both crystals, the total energies calculated by the DPSI bases are much lower than those by the PSI bases, and are very close to the PW results. The figure visually shows the advantages of the DPSI bases over the PSI bases.

The total energies of 26 crystals are presented in Table VI for both the PSI and DPSI bases. The MAE of DZP-DPSI

TABLE IX. Bulk moduli (in GPa) of 26 solids at their equilibrium lattice constants obtained from various LCAO basis sets, compared to the PW results.

	PSI				DPSI				
	DZ	DZP	TZDP	QZTP	DZ	DZP	TZDP	QZTP	PW
AlAs	55.34	66.02	65.38	66.54	63.05	66.82	66.39	66.29	67.03
AlNw	180.84	190.27	192.06	194.30	176.98	188.59	191.53	190.84	194.27
AlP	70.50	78.98	79.74	80.02	75.57	81.45	81.50	81.55	82.37
AlSb	44.93	49.04	49.30	49.51	46.53	49.52	48.98	49.00	49.41
BN	368.18	369.67	369.42	369.45	365.48	368.43	369.61	369.25	368.49
BP	156.43	157.16	155.95	155.89	151.56	160.78	160.35	160.45	160.28
C	426.23	433.13	433.00	431.36	420.91	432.46	430.59	430.47	430.21
CdSew	43.82	44.91	44.93	45.29	43.84	44.44	44.63	44.94	44.77
CdSw	52.21	52.68	53.29	53.29	52.68	53.15	53.25	53.55	53.40
CdTe	34.27	35.24	34.93	34.73	34.82	35.13	35.00	35.04	35.18
GaAs	54.16	57.46	56.68	56.94	57.74	59.78	59.38	59.39	59.81
GaN	165.61	166.93	168.52	169.20	168.48	171.19	171.69	171.29	172.18
GaP	66.15	71.62	73.43	73.58	71.54	75.98	76.00	76.02	76.58
GaSb	42.57	42.67	42.62	43.69	44.09	44.80	44.62	44.60	44.59
InP	59.65	61.97	61.77	60.49	56.86	59.22	59.29	59.45	59.21
LiF	61.91	66.06	66.54	66.78	61.56	67.30	65.54	66.54	67.74
MgO	148.16	145.78	148.99	149.03	153.36	148.97	148.45	146.26	151.65
MgS	70.07	73.75	73.80	74.71	70.71	74.57	74.67	74.85	75.20
NaCl	23.02	22.75	23.52	23.43	23.01	23.10	23.25	23.46	23.75
Si	81.11	94.52	90.79	90.32	76.94	88.00	86.61	86.34	87.52
SiC	173.47	210.52	210.70	209.79	176.14	210.64	210.21	209.55	210.90
ZnO	125.76	125.93	128.89	128.22	127.34	128.71	128.93	130.14	129.09
ZnOw	127.23	127.52	130.04	130.03	128.46	130.02	129.98	131.31	130.44
ZnS	64.80	66.84	68.81	69.52	65.60	68.33	68.75	68.97	69.73
ZnSe	53.60	54.27	54.07	56.15	54.81	55.33	56.31	56.42	56.95
ZnTe	41.62	41.71	42.67	42.61	42.24	43.04	43.44	43.48	43.38
MAE	5.97	2.54	2.02	1.71	5.28	0.98	0.85	0.98	
MRE	6.17%	2.92%	2.25%	1.84%	4.70%	1.04%	0.91%	0.91%	

bases (with respect to the PW reference results) is 0.15 eV, which is much smaller than the 0.36 eV of the DZP-PSI bases, and even smaller than 0.22 eV of the much larger QZTP-PSI bases.

2. Lattice constants

Table VII lists the lattice constants of the 22 fcc crystals. For clarity of the table, four crystals with the wurtzite structure (AlNw, CdSew, CdSw, and ZnOw), which each have two lattice constants, are omitted. The lattice constants are fitted by the Birch-Murnaghan equation of state [25].

Again, for nearly all crystals, the DPSI bases show better performance than the PSI bases. The MAE and MRE of the DPSI bases are approximately only half of those of the corresponding PSI bases of the same level, and the quality of the DZP-DPSI bases is comparable to the QZTP-PSI bases.

3. Cohesive energies

The cohesive energies are presented in Table VIII. For most of the crystals, the errors of the DPSI bases are smaller than those of the PSI bases. The MAE of DZP bases is reduced from 0.15 eV to 0.09 eV. Increasing the size of the bases does not significantly improve the results, which, according to the results of the molecules, suggests that the accuracy is approaching the limit of the NAO bases at the given cutoff radii and highest angular momentum of the NAOs.

4. Bulk moduli

The bulk moduli of 26 crystals calculated using various NAO basis sets as well as using the PW bases are presented in Table IX. The DPSI DZP bases show a MAE of 0.98 GPa, compared to a MAE of 2.54 GPa of the PSI DZP bases and 1.71 GPa of the PSI QZTP bases. It is worth noting that, however, for DPSI bases the accuracy of the calculated bulk moduli does not show systematic improvement beyond the DZP basis set. Thus a MAE of ~0.98 GPa might be the upper limit of such a numerical orbital method.

5. Band structures

In this subsection, we check the influence of the type of NAO bases on the band structure calculations. In Fig. 3, the PBE band structures of Si crystal calculated using both PSI [blue solid lines in panel (a)] and DPSI [blue solid line in panel (b)] DZP basis sets are presented. For comparison, the results calculated using the PW bases are plotted in both panels of Fig. 3 (the red dashed lines) as well.

The indirect band gap of Si calculated using the PW basis set is 0.552 eV. If the PSI DZP basis set is used, the obtained

TABLE X. Band gap (in eV) of 26 solids obtained from various LCAO basis sets, compared to the PW. For each material, the same structure is used for all bases. The band gap is calculated in an $8 \times 8 \times 8$ **k** mesh.

	PSI				DPSI				
	DZ	DZP	TZDP	QZTP	DZ	DZP	TZDP	QZTP	PW
AlAs	1.553	1.472	1.433	1.386	1.564	1.484	1.412	1.410	1.408
AlNw	3.860	4.173	4.187	4.168	3.835	4.163	4.187	4.189	4.146
AlP	2.150	1.642	1.588	1.549	1.944	1.644	1.569	1.569	1.572
AlSb	1.187	1.318	1.287	1.249	1.251	1.282	1.241	1.241	1.224
BN	5.036	4.692	4.547	4.548	4.803	4.592	4.548	4.545	4.543
BP	2.033	1.398	1.311	1.305	1.698	1.335	1.321	1.317	1.304
C	4.418	4.289	4.185	4.183	4.435	4.265	4.197	4.195	4.176
CdSew	0.665	0.623	0.625	0.626	0.672	0.680	0.661	0.667	0.665
CdSw	1.100	1.061	1.082	1.081	1.102	1.080	1.101	1.101	1.111
CdTe	0.761	0.731	0.747	0.740	0.761	0.745	0.767	0.764	0.766
GaAs	0.324	0.369	0.386	0.374	0.501	0.519	0.487	0.473	0.463
GaN	1.725	1.644	1.665	1.639	1.880	1.749	1.728	1.727	1.722
GaP	1.773	1.660	1.631	1.608	1.926	1.702	1.662	1.660	1.648
GaSb	0.164	0.108	0.043	0.085	0.175	0.129	0.124	0.122	0.120
InP	0.700	0.665	0.627	0.620	0.761	0.729	0.703	0.697	0.687
LiF	9.102	9.214	9.243	9.225	8.914	9.124	9.145	9.188	9.248
MgO	4.644	4.701	4.694	4.701	4.625	4.680	4.699	4.708	4.758
MgS	3.268	2.798	2.774	2.766	3.201	2.779	2.780	2.788	2.832
NaCl	5.055	5.070	5.084	5.081	5.038	5.064	5.079	5.090	5.114
Si	1.100	0.744	0.600	0.586	0.940	0.638	0.609	0.604	0.592
SiC	2.180	1.478	1.375	1.368	2.092	1.450	1.369	1.373	1.386
ZnO	0.722	0.698	0.702	0.710	0.744	0.721	0.729	0.731	0.736
ZnOw	0.847	0.834	0.843	0.848	0.864	0.854	0.861	0.864	0.868
ZnS	1.894	1.881	1.907	1.917	1.946	1.937	1.944	1.946	1.941
ZnSe	1.243	1.203	1.212	1.227	1.301	1.321	1.275	1.286	1.274
ZnTe	1.229	1.188	1.221	1.228	1.271	1.247	1.255	1.256	1.247
MAE	0.2000	0.0689	0.0372	0.0356	0.1755	0.0462	0.0204	0.0157	
MRE	17.124%	8.720%	5.453%	5.667%	12.649%	3.550%	1.328%	0.955%	

band gap is 0.713 eV, yielding a relative error up to nearly 30%. In contrast, with the DPSI DZP basis set, the calculated band gap is 0.605 eV, corresponding to a much reduced relative error of 10%.

For more quantitative information, we measure the difference between two band structures by taking the root mean square deviation, i.e.,

$$\delta E_{\text{band}} = \frac{1}{N_{\text{b}} N_k} \sqrt{\sum_{\mathbf{k}} \sum_{n=1}^{N_{\text{b}}} \left| \varepsilon_{n\mathbf{k}}^{\text{NAO}} - \varepsilon_{n\mathbf{k}}^{\text{PW}} \right|^2}, \tag{12}$$

where N_{b} is the number of bands. Here we include the lowest seven bands in the definition of Eq. (12), covering the valence bands and low-lying conduction bands, which the DZP bases are supposed to describe. According to this definition, the deviation of the band structure calculated by the PSI bases is 0.0093 eV, which is reduced to 0.0050 eV if one turns to the DPSI bases. It can be seen from Fig. 3 that the band lines calculated by the DPSI basis [panel (b)] are in better agreement with the PW reference results than those calculated by the PSI bases [panel (a)].

TABLE XI. Properties of Si crystal calculated using PSI and DPSI bases with different cutoff radii, compared with PW results. The DZP bases are used in the LCAO calculations.

	PSI			DPSI			PW
R_c (Bohr)	6	7	8	6	7	8	
Total energies (eV)	1.98	1.03	0.42	0.45	0.17	0.11	0.00
Cohesive energies (eV)	11.46	9.88	9.21	9.93	9.28	9.03	8.98
Lattice constant (Å)	5.470	5.506	5.492	5.458	5.484	5.481	5.476
Bulk moduli (GPa)	125.32	114.06	94.52	91.04	90.29	88.00	87.52
Band gap (eV)	1.34	0.93	0.74	0.69	0.69	0.64	0.59

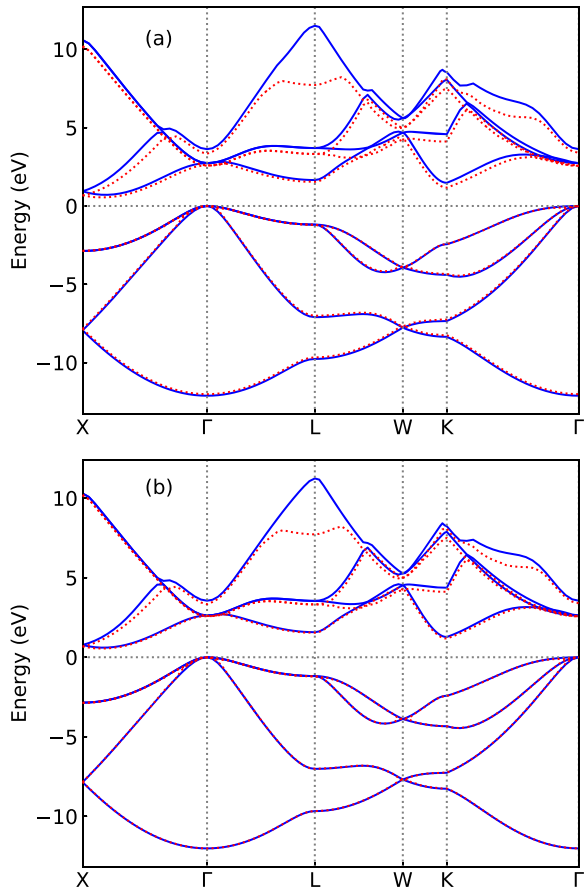

FIG. 3. Comparison of the band structures of Si crystal calculated by different NAO bases (blue solid lines) and the PW basis (red dashed lines). The NAO results in panel (a) are obtained using the PSI bases, whereas those in panel (b) are obtained using the DPSI bases.

The band gaps of 26 crystals are presented in Table X. For simplicity, the band gaps in the table are obtained via the difference between the conduction band minimum and valence band maximum on an $8 \times 8 \times 8$ **k**-point mesh, which may be slightly different from the band gaps calculated along the high-symmetry **k**-point paths.

From Table X, it is evident that the band gaps calculated using the DPSI bases are superior to those by the PSI bases. Specifically the MAE of DPSI DZP is smaller than that of PSI DZP and the MRE of DPSI DZP is even smaller than that of PSI QZTP.

C. Cutoff radii of the NAOs

It has been shown in Ref. [8] that increasing the cutoff radii of the NAOs can improve the quality of the bases, which, however, is computationally more costly. To examine how the total energy converges with respect to the cutoff radii of NAOs, we show in Fig. 4 the total energies of Si crystal as a function of the NAO radius for both the PSI and DPSI bases. As shown in the figure, the total energies calculated using the DPSI bases converge much faster upon increasing radius than those of the PSI bases. Specifically, the total energies calculated by DPSI bases converge to a high precision already

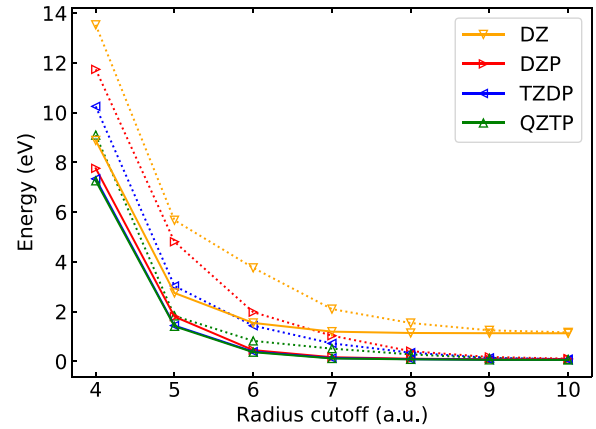

FIG. 4. Differences between the total energies calculated using NAOs and that of the PW results as a function of the NAO cutoff radii. The test system is Si crystal in diamond structure. The solid lines represent the DPSI results, whereas the dotted lines represent the PSI ones.

at about $R_c = 7$ Bohr, whereas one needs to go to 10 Bohr for the PSI bases to achieve a similar level of precision. To further illustrate the effects of NAO radii, we compare in Table XI the total energy, cohesive energy, lattice constant, bulk modulus and band gap of Si crystal calculated by the DZP-PSI and DZP-DPSI bases with different R_c. We see that, for DZP-PSI bases, the errors are huge for $R_c \leqslant 7$ Bohr, and $R_c = 8$ Bohr is needed to obtain accurate results. In contrast, for the DZP-DPSI bases, one is able to obtain satisfactory results even for $R_c = 6$ Bohr, which are comparable in precision to the results calculated by the DZP-PSI base with $R_c = 8$ Bohr. Reducing the radii of the NAOs without sacrificing accuracy can greatly save computational time and memory consumption in the electronic calculations.

IV. SUMMARY

We propose a scheme to construct high-quality NAO basis sets for density-functional calculations. Compared to the original CGH scheme proposed in Ref. [8], the key additional ingredient of this scheme is that the derivatives of the wavefunctions are also incorporated in the optimization procedure. This scheme not only simplifies the procedures of the original scheme, but also greatly improves the quality of the generated NAO base sets. The relatively small DZP bases, most often used for production calculations, already yield remarkable accuracy in the calculation of the structural and electronic properties of molecules and crystals. With suitably chosen radii of the NAOs, the numerical precision achieved by the much smaller DZP bases generated via this scheme are comparable to that of the QZTP bases generated via the original scheme.

ACKNOWLEDGMENTS

This work was funded by the National Key Research and Development Program of China (Grant No. 2016YFB0201202) and the Chinese National Science Foundation, Grants No. 11774327 and No. 11874335. The numerical calculations were done on the USTC HPC facilities.

TABLE XII. Absolute errors of the individual components of the total energy obtained using the DZP-PSI (left side) and DZP-DPSI (right side) bases with respect to the jY reference results for a set of molecules, obtained after the first iteration of the calculations.

	PSI						DPSI					
	E_{tot}	E_{T}	E_{H}	E_{xc}	$E_{\text{ps-l}}$	$E_{\text{ps-nl}}$	E_{tot}	E_{T}	E_{H}	E_{xc}	$E_{\text{ps-l}}$	$E_{\text{ps-nl}}$
Br_2	0.11	0.40	0.33	0.02	0.31	0.23	0.05	0.16	0.48	0.02	0.53	0.22
Cl_2	0.08	0.35	0.37	0.01	0.30	0.14	0.06	0.32	0.38	0.01	0.26	0.08
CO	0.09	0.84	0.82	0.15	1.56	0.31	0.07	0.22	0.47	0.07	0.86	0.35
F_2	0.06	0.85	0.48	0.08	0.71	0.30	0.04	0.53	0.46	0.05	0.62	0.22
I_2	0.24	0.72	0.55	0.05	0.78	0.56	0.05	0.86	1.41	0.09	1.93	0.25
Li_2	0.32	1.89	0.39	0.13	0.65	0.91	0.03	0.97	0.22	0.05	0.18	0.61
LiH	0.02	0.47	0.26	0.02	0.21	0.38	0.01	0.16	0.35	0.06	0.36	0.24
N_2	0.02	1.11	1.34	0.25	2.24	0.49	0.01	0.61	1.32	0.25	2.04	0.73
Na_2	0.03	10.77	4.88	1.02	7.21	5.97	0.13	9.74	5.81	1.00	7.93	5.37
O_2	0.10	0.76	0.26	0.01	0.23	0.63	0.07	0.80	0.21	0.00	0.15	0.63
S_2	0.13	0.64	0.31	0.01	0.32	0.50	0.06	0.45	0.44	0.02	0.41	0.38
MAE	0.11	1.71	0.91	0.16	1.32	0.95	0.05	1.35	1.05	0.15	1.39	0.83

APPENDIX: ERROR ANALYSIS OF INDIVIDUAL COMPONENTS OF THE TOTAL ENERGY

In order to gain a deeper insight into the origin of the advantage of the DSPI bases over the standard PSI bases, we performed an error analysis of the individual components of the total energy. To this end, the ground-state total energy is decomposed into five terms,

$$E_{\text{tot}} = E_{\text{T}} + E_{\text{H}} + E_{\text{xc}} + E_{\text{ps-l}} + E_{\text{ps-nl}}, \tag{A1}$$

including the kinetic energy, the Hartree energy, the exchange-correlation energy, and the potential energies due to the local and nonlocal parts of the pseudopotentials. What is presented in Tables XII and XIII are the (absolute) errors of each term, for a set of molecules, obtained by the DZP-PSI and DZP-DPSI bases with respect to the jY reference results. Specifically, Tables XII and XIII show the errors obtained after the first iteration and at full self-consistency of the calculations, respectively.

This analysis reveals that, for most of the molecules, the initial basis set incompleteness error of the kinetic energy is substantially reduced when going from the PSI to DSPI basis prescription (cf. MAEs in Table XII), whereas other parts do not show this improvement. This behavior is understandable since the DPSI basis functions by construction have improved gradients and hence feature a better-quality kinetic energy. Compared to the kinetic energy, other parts of the total energy are not so sensitive to the wavefunction gradients as the kinetic energy is and hence do not show similar improvement initially. However, as the self-consistency process goes on, the variational principle of the DFT total energy calculation drives the improved accuracy of the kinetic energy transferring to other parts of the total energy. Eventually, one can observe from Table XIII that, on average, not only the kinetic energy, but also other parts of the total energy get improved, but the magnitude of the kinetic energy improvement is not as big as what happened initially.

TABLE XIII. Absolute errors of the individual components of the total energy obtained using the DZP-PSI (left side) and DZP-DPSI (right side) bases with respect to the jY reference results for a set of molecules, obtained after the full self-consistency of the calculations is achieved.

	PSI						DPSI					
	E_{tot}	E_{T}	E_{H}	E_{xc}	$E_{\text{ps-l}}$	$E_{\text{ps-nl}}$	E_{tot}	E_{T}	E_{H}	E_{xc}	$E_{\text{ps-l}}$	$E_{\text{ps-nl}}$
Br_2	0.13	0.45	0.21	0.05	0.13	0.20	0.05	0.29	0.27	0.03	0.24	0.18
Cl_2	0.10	0.47	0.25	0.04	0.11	0.03	0.07	0.48	0.21	0.04	0.23	0.06
CO	0.16	0.38	0.16	0.04	0.84	0.51	0.13	0.85	0.79	0.17	1.96	0.62
F_2	0.09	1.03	0.31	0.10	0.66	0.41	0.06	0.93	0.18	0.08	0.44	0.39
I_2	0.28	1.30	1.06	0.08	2.44	0.16	0.06	1.23	2.01	0.20	3.56	0.45
Li_2	0.36	0.53	0.73	0.14	0.99	0.29	0.00	0.19	0.16	0.04	0.24	0.08
LiH	0.12	0.19	0.23	0.08	0.25	0.17	0.05	0.13	0.08	0.02	0.14	0.08
N_2	0.09	0.17	0.49	0.10	0.41	0.13	0.07	0.28	0.38	0.08	0.09	0.00
Na_2	0.12	1.88	2.95	0.34	3.58	0.97	0.02	1.20	0.63	0.16	0.98	0.66
O_2	0.15	1.13	0.37	0.02	0.25	0.39	0.10	1.20	0.16	0.01	0.65	0.28
S_2	0.17	0.57	0.12	0.02	0.60	0.33	0.08	0.42	0.17	0.01	0.66	0.48
MAE	0.16	0.74	0.63	0.09	0.93	0.33	0.06	0.66	0.46	0.08	0.83	0.30

[1] B. Delly, J. Chem. Phys. **113**, 7756 (2000).
[2] J. M. Soler, E. Artacho, J. D. Gale, A. García, J. Junquera, P. Ordejón, and D. Sánchez-Portal, J. Phys.: Condens. Matter **14**, 2745 (2002).
[3] K. Koepernik and H. Eschrig, Phys. Rev. B **59**, 1743 (1999).
[4] V. Blum, R. Gehrke, F. Hanke, P. Havu, V. Havu, X. Ren, K. Reuter, and M. Scheffler, Comput. Phys. Commun. **180**, 2175 (2009).
[5] T. Ozaki, Phys. Rev. B **67**, 155108 (2003).
[6] O. F. Sankey and D. J. Niklewski, Phys. Rev. B **40**, 3979 (1989).
[7] J. Junquera, O. Paz, D. Sanchez-Portal, and E. Artacho, Phys. Rev. B **64**, 235111 (2001).
[8] M. Chen, G. Guo, and L. He, J. Phys.: Condens. Matter **22**, 445501 (2010).
[9] D. S. Portal, E. Artacho, and J. M. Soler, Solid State Commun. **95**, 685 (1995).
[10] D. S. Portal, E. Artacho, and J. M. Soler, J. Phys.: Condens. Matter **8**, 3859 (1996).
[11] P. Li, X. Liu, M. Chen, P. Lin, X. Ren, L. Lin, C. Yang, and L. He, Comput. Mater. Sci. **112**, 503 (2016).
[12] E. Anglada and J. M. Soler, Phys. Rev. B **73**, 115122 (2006).
[13] Y. Liu, X. Ren, and L. He, J. Chem. Phys. **151**, 215102 (2019).
[14] X. Liu, D. Zheng, X. Ren, L. He, and M. Chen, J. Chem. Phys. **147**, 064505 (2017).
[15] Q. Wang, D. Zheng, L. He, and X. Ren, Phys. Rev. Applied **12**, 044060 (2019).
[16] X. Liu, Y. Qi, D. Zheng, C. Zhou, L. He, and F. Huang, Geochim. Cosmochim. Acta **223**, 364 (2018).
[17] Y. Zheng, L. Liu, H. Nan, Z. X. Shen, and H. Zhuang, Sci. Adv. **6**, eaba0826 (2020).
[18] A. Paszke, S. Gross, F. Massa, A. Lerer, J. Bradbury, G. Chanan, T. Killeen, Z. Lin, N. Gimelshein, L. Antiga *et al.*, Adv. Neur. Inf. Process. Syst. **32**, 7994 (2019).
[19] D. P. Kingma and J. Ba, Adam: A method for stochastic optimization, arXiv:1412.6980.
[20] S. D. Kenny, A. P. Horsfield, and H. Fujitani, Phys. Rev. B **62**, 4899 (2000).
[21] M. Schlipf and F. Gygi, Comput. Phys. Commun. **196**, 36 (2015).
[22] J. P. Perdew, K. Burke, and M. Ernzerhof, Phys. Rev. Lett. **77**, 3865 (1996).
[23] D. Vanderbilt, Phys. Rev. B **41**, 7892 (1990).
[24] D. R. Hamann, Phys. Rev. B **88**, 085117 (2013).
[25] F. Birch, Phys. Rev. **71**, 809 (1947).